Available online at www.sciencedirect.com
ScienceDirect
Engineering Structures 30 (2008) 1647–1658
ENGINEERING STRUCTURES
www.elsevier.com/locate/engstruct

Behaviour of steel beam to concrete-filled SHS column frames: Finite element model and verifications

Lin-Hai Han[a,b,*], Wen-Da Wang[a,c], Xiao-Ling Zhao[b]

[a] *Department of Civil Engineering, Tsinghua University, Beijing, 100084, China*
[b] *Department of Civil Engineering, Monash University, Clayton, VIC 3168, Australia*
[c] *College of Civil Engineering, Lanzhou University of Technology, Lanzhou, 730050, China*

Received 19 July 2007; received in revised form 27 October 2007; accepted 31 October 2007
Available online 20 December 2007

Abstract

This paper presents the behaviour of the composite frame with concrete-filled square hollow section (SHS) columns to steel beam. Finite element modeling (FEM) was developed to carry out the behaviour of composite frames under a constant axial load on columns and a lateral cyclic load on the frame. Accurate material and geometrical nonlinear for confined concrete and steel were considered in the analysis. The finite element program ABAQUS was adopted. A damage plastic model for concrete and elasto-plastic model for steel were used respectively. Six composite frame tests were carried out to verify the FE model. Each test frame specimen consisted of two concrete-filled SHS columns and a steel beam to represent an interior frame in a building. The results obtained from the finite element model were verified against those obtained from the experimental results.

Keywords: Concrete-filled steel tubular (CFST) column; Beam; Composite frame; Concrete; Confinement; Finite element model (FEM); Mechanical behaviour; Ductility; Energy dissipation

1. Introduction

Concrete-filled steel tubular (CFST) columns are being increasingly used in the construction of buildings due to their excellent static and earthquake-resistant properties such as high strength and stiffness, high ductility, and large energy absorption capacity.

There have been a large number of research studies on the realistic performance of concrete-filled steel tubular singular columns. Several state of the art reports or papers were published recently on CFST structures, such as Shams et al. [1], Shanmugam et al. [2], Gourley et al. [3] and Nishiyama et al. [4]. Research on CFST beams has been reported in Zhao et al. [5], Elchalakani et al. [6,7]. Little research has been done to investigate the behaviour on the frame of this type of construction, especially the theoretical research by accurate model.

Kawaguchi et al. [8] tested four portal frame specimens consisting of concrete-filled square hollow section (SHS) steel tubular columns and an H-shaped steel beam with through-type diaphragms under the constant axial load and cyclic horizontal load. It is concluded that CFST frame has excellent earthquake resistance. The axial load level of columns is generally small, the maximum value is 0.3 or so. Matsui [9] carried out tests of square CFST frames with changing width-to-thickness ratio of the column tube, diaphragm type, and loading histories, and which had ultimate failure in the column. It is concluded that the CFST frame showed excellent horizontal load carrying capacity and the limit value of the width-to-thickness ratio of the CFST column could be magnified to about 1.5 times that for the unfilled tubes due to the effects of the in-filled concrete on the local buckling strength and post buckling behaviour of the tube. Tsai et al. [10] completed a pseudo-dynamic test of a full-scale 3-story 3bay composite frame using CFST columns and

* Corresponding author at: Department of Civil Engineering, Tsinghua University, Beijing, 100084, China. Tel.: +86 10 62797067; fax: +86 10 62781488.
E-mail addresses: lhhan@tsinghua.edu.cn (L.-H. Han), wdwang@tsinghua.edu.cn (W.-D. Wang), zxl@eng.monash.edu.au (X.-L. Zhao).

0141-0296/$ - see front matter © 2007 Elsevier Ltd. All rights reserved.
doi:10.1016/j.engstruct.2007.10.018

Notations

A_s	Steel cross-sectional area
A_c	Concrete cross-sectional area
b_f	Overall width of I-beam
B	Sectional dimension
E_a	Dissipated energy ability
E_c	Concrete modulus of elasticity
E_s	Steel modulus of elasticity
f'_c	Concrete cylinder compressive strength
f_{cu}	Concrete cube compressive strength
f_{ck}	Concrete axial compressive strength
f_y	Yield stress of steel
f_u	Ultimate strength of steel
h	Overall height of I-beam
h_e	Equivalent damping coefficient
H	Height of column of composite frame
k	Beam-to-column linear stiffness ratio
L	Length of beam of composite frame
n	Axial load level
N_o	Axial load of CFST column
N_u	Ultimate compression resistance of composite section
P	Lateral load of frame
P_u	Estimated ultimate lateral load capacity of frame
P_{ue}	Ultimate lateral load capacity of frame by experiment
P_{ua}	Ultimate lateral load capacity of frame by ABAQUS
P_y	Yield lateral load of frame
$P_{85\%}$	85% of ultimate lateral load capacity (P_{ue})
r	Radius of the corner of SHS cold-formed steel tube
t_f	Flange thickness of I-beam
t_s	Wall thickness of the steel tube
t_w	Web thickness of I-beam
w	Thickness of SHS steel tube
α	Steel ratio ($=A_s/A_c$)
σ	Stress
ε	Strain
ε_y	Yield strain
ν_s	Poisson's ratio of steel
ν_c	Poisson's ratio of concrete
Δ	Lateral displacement of frame
Δ_u	Lateral displacement when lateral load of frame falls 85% of P_{ue}
Δ_y	Yield displacement of frame
μ	Displacement ductility coefficient

steel beams with buckling restrained braces in the middle span, and the test result showed the excellent seismic ability of the composite frame. Muhummud [11] and Herrera [12] predicted the seismic behaviour of multi-story CFST composite frame using the nonlinear dynamic time history analysis software DRAIN-2DX, which was based on the fiber beam–column element theory.

Little success has been achieved so far in developing an accurate model due to the complexity in modeling the concrete confinement effect for concrete-filled steel tubular members. Schneider [13] developed a three-dimensional nonlinear finite element model for concrete-filled tubular columns by the ABAQUS program. The unconfined uniaxial stress–strain curve for concrete provided in the ABAQUS material library was used as five segments linear curves. Hu et al. [14] developed a nonlinear finite element model using the ABAQUS to simulate the behaviour of concrete-filled steel tube columns. The concrete confinement was achieved by matching the numerical results by trial and error via parametric study. Hu et al. [15] analyzed concrete-filled tubular columns subjected to an axial compressive force and bending moment in combination by using the ABAQUS, the material constitutive models are same as Hu et al. [14]. Ellobody and Young [16] analyzed the behaviour of normal and high strength concrete-filled tubular columns using the ABAQUS, where the concrete model and the other parameters were the same as Hu et al. [14]. Han et al. [17] presented a uniaxial compression stress–strain relation for confined core concrete of CFST member for ABAQUS, and the plastic damage concrete model was used to simulate the core concrete. With the model, the load versus deformation relationship was predicted. The experimental results matched well with the results that obtained from the finite element model using ABAQUS.

Set against this background, the authors have recently been engaged in research studies to determine the mechanical behaviour of the composite frames with concrete-filled square hollow section (SHS) steel tubular columns to steel beam. Both theoretical and experimental studies have been carried out. The main objective of this study is to develop an accurate finite element model to simulate the behaviour of the composite frames with concrete-filled square hollow section (SHS) steel tubular columns to steel beam. The finite element program ABAQUS [18] was used in the analysis. The effects of concrete strength and concrete confinement were considered in the analysis. The interface between concrete and the steel tube was also modeled. To validate the FEA model, this paper presents new test data pertaining to the behaviour of CFST column to steel beam frames. In the experimental study, six tests were performed and the test parameters included the cross-sectional dimension, the axial load level, and the beam–column linear stiffness ratio. Each test specimen consisted of two CFST columns and a steel beam to represent a typical frame element in a building, and each specimen was tested under a constant axial load and a cyclically increasing lateral load. Comparisons between the FEA predicted results and the experimental results indicate that the suitability of the FEA model to predict the P–Δ relations of steel beam to CFST column frames.

2. Finite element modeling

2.1. General descriptions

In order to accurately simulate the actual behaviour of frames with concrete-filled steel tube (CFST) square columns

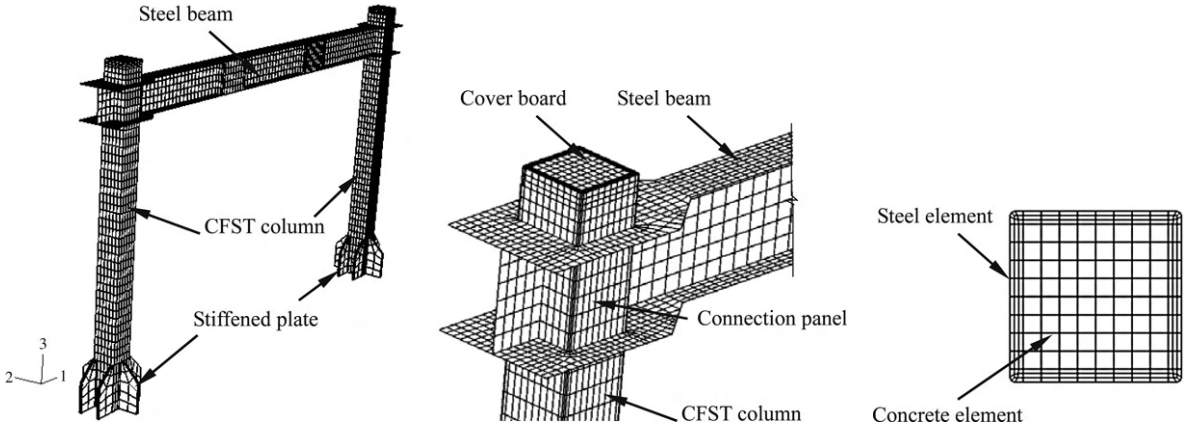

(a) The whole FEA model. (b) Steel beam discretization. (c) Section discretization.

Fig. 1. Typical finite element model of composite CFST frames.

to steel beam, the main five components of the frames need to be modeled. These components are the confined concrete of square columns, the interface and contact between the concrete and the steel tube, the steel tube, the connection details between columns to steel beam, and the steel beam. In addition to these parameters, the choice of the element type, mesh size, boundary conditions and load applications that provide accurate and reasonable results are also important in simulating the behaviour of structural frames. Han et al. [17] simulated the performance of concrete-filled thin-walled steel tubes under pure torsion by ABAQUS, and some analysis strategy, such as material modeling of core concrete and steel tubes was described. This paper shows some key issues for analyzing composite frames using ABAQUS. The FE results are presented in Figs. 6, 12 and 13, that will be verified later in the paper.

2.2. Finite element type and mesh

Different element types have been tried in order to find a suitable element to simulate the behaviour of frames. Solid elements were found to be more efficient in modeling the concrete as well, and steel tubes were modeled with shell elements. A fine mesh of three-dimensional eight-node linear brick and reduced integration with hourglass control solid element (C3D8R) is used for concrete and four-node doubly curved general-purpose shell with finite membrane strain shell element (S4) is used for steel tubes and steel beam. Different mesh sizes were tried in order to find a reasonable mesh that provides both accurate results and less computational time. It is found that a mesh size of 1 (length):1 (width):2 (depth) approximately for solid elements and 1 (length):1 (width) approximately for shell elements, can achieve accurate results. Typical meshes of composite frames are shown in Fig. 1(a)–(c), respectively. Fig. 1(b) shows typical steel beam elements and Fig. 1(c) shows the section elements discretization in the FEA model. A typical joint, which consists of a concrete-filled steel tubular (CFST) column, a steel beam and the outer ring, shown in Fig. 1(b), is used in the analysis. These kinds of joints have been widely used in tall buildings in China.

2.3. Boundary conditions and load application

The bottom surfaces of the concrete-filled steel tube columns were fixed against all degrees-of-freedom. The top of CFST columns supported constant axial load and the steel beam were subjected to a cyclically increasing flexural load. The axial loads of CFST columns were applied in increment using *LOAD option available in the ABAQUS library, and the horizontal load of the steel beam end was applied in an appointed displacement using boundary condition under different increment steps. The axial force is transferred to the composite column by an elastic rigid plate whose modulus of elasticity is 10^{12} N/mm^2 and Poisson's ratio is 0.0001. The load step and displacement step were solved using static and general arithmetic with geometrical and material nonlinear methods available in the ABAQUS library.

2.4. Material modeling of steel

The elastic–plastic material behaviour provided by ABAQUS (using the *PLASTIC option) allows a multi-linear or bilinear stress–strain curve to be used. The steel beam and SHS steel tubes were simulated by this model. The first part of the multi-linear curve represents the elastic part up to the proportional limit stress with a measured modulus of elasticity (E_s) and Poisson's ratio (ν_s) equal to 0.3. The Mises yield surface is used to define isotropic yielding for steel material and the model for steel assumes associated plastic flow. The model parameters for the bilinear stress–strain curve are yield strength (f_y), the modulus of elasticity (E_s) and the tangent moduli ($E'_s = 0.01E_s$). The magnitude of the modulus of elasticity (E_s) is equal to 206,000 N/mm^2.

For cold-formed steel tubes, different strength and residual stresses for corner zone and flat zone, should be considered. The techniques used in the manufacture of cold-formed sections induce substantial changes on the mechanical characteristics, and also result in cold-formed residual stresses. An idealized multi-linear stress–strain model for cold-formed steel SHS steel tube is adopted in this paper. This model was developed by Abdel-Rahman and Sivakumaran [19], where a cold-formed

section is divided into two zones: a corner zone and a flat zone, and the strength of a corner zone and a flat zone are different. Sully and Hancock [20] proposed that a residual stress of $0.4f_y$ be used for the corner zones, and a residual stress of $(0.24 - 0.0006w)f_y$ be used for the flat zone. Where f_y is the yield strength in unit N/mm^2 and w is the thickness of SHS steel tube in unit mm, respectively. The residual stress has a linear variation through the section thickness, with tensile stress on the outer surface, and equal compressive stress on the inside surface at the same location. Residual stress is considered in ABAQUS by *INITIAL CONDITIONS options and defined as TYPE = STRESS.

2.5. Material modeling of core concrete

Han et al. [17,21] gave a practical and accurate model for core concrete of CFST member using ABAQUS. This paper used the material model to simulate the core concrete of the composite columns in a frame.

The damaged plastic model is adopted to simulate the concrete provided by the ABAQUS library. The model allows to input a multi-linear uniaxial compression stress–strain curve. The other parameters, such as dilation angle, eccentricity, ratio of the biaxial compression strength to uniaxial compression strength of concrete, the ratio of the second stress invariant on the tensile meridian to that on the compressive meridian, viscosity parameter, etc., are default by ABAQUS [18]. The modulus of elasticity (E_c) of concrete is equal to $4730\sqrt{f'_c}$ by ACI 318 [22], where f'_c means the cylinder compression strength of concrete. The Poisson's ratio (ν_c) is equal to 0.2. The plastic-damage model uses a yield condition based on the yield function proposed by Lubliner et al. [23] and incorporates the modifications proposed by Lee and Fenves [24] to account for the different evolution of strength under tension and compression. The plastic-damage model for concrete assumes non-associated potential flow rule.

Tension stiffening is required in the damaged plasticity model of concrete. The tension stiffening can be specified by means of a post-failure stress–strain relation or by applying a fracture energy cracking criterion in ABAQUS. When there is no reinforcement in significant regions of the model, the tension stiffening approach described with stress–strain relation will introduce unreasonable mesh sensitivity into the results. However, it is generally accepted that Hillerborg's [25] fracture energy proposal is adequate to allay the concern for many practical purposes, thus the model was used in the analysis on CFST members [17,21], which is also used in this paper.

2.6. Concrete–steel tube interface

The contact between the concrete and the steel tube is modeled by interface elements. The interface elements consist of two matching contact surfaces of concrete and steel tube elements. The normal direction of the two surfaces is hard contact and the tangent contact is simulated by the Coulomb friction model. The friction between the two contact surfaces is maintained as long as the faces remain in contact. The coefficient of friction between the two surfaces is taken as 0.6 in the analysis from Han et al. [17]. The interface element allows the surfaces to separate under the influence of a tensile force. However, the two contact elements are not allowed to penetrate each other.

The I-shaped steel beam is welded from the three pieces of rectangular steel plate. The *TIE option in ABAQUS is used to simulate the welding lines of steel beam. The connection of CFST columns to beam are also welded, so those welding lines are simulated by *TIE command in ABAQUS.

3. Frame tests

A series of tests on composite frames with steel beam to CFST columns were conducted by the authors [26], the test results are used to verify the FEA model presented in the paper.

3.1. Specimen preparation

Six concrete-filled SHS columns to steel composite frame specimens were tested under a constant axial load and a cyclically increasing lateral load. Fig. 2 shows the test frame configuration. The column height was 1450 mm, the steel beam span was 2500 mm, as shown in Fig. 3. The frame specimens were designed using the concept of strong-column–weak-beam, so beam failure mode was expected.

The following two parameters, which are important for the design of a frame structure, were selected in the current test programming, i.e.

- Level of axial load in the column, n ($\approx$0, 0.3 and 0.6), which is defined as $n = N_o/N_u$, where N_o is the axial load applied in the column and N_u is the axial compressive capacity of the column and N_u was determined by specification Eurocode 4 [27].
- The beam–column linear stiffness ratio k (=0.34–0.62), where k is defined as i_b/i_c, where i_b and i_c are the linear stiffnesses of beam and column, respectively. i_b is defined as E_sI_b/L, where I_b is the moment of inertia for steel beam, E_s is the modulus of elasticity of steel and L is the length of beam, respectively. i_c is defined as EI_c/H, where H is the height of column. The stiffness of concrete-filled SHS steel tube column is $EI_c = E_sI_s + 0.6E_cI_c$, where E_s and E_c are the modulus of elasticity of steel and concrete, respectively, and I_s and I_c are the moment of inertia for hollow steel cross-section and core concrete cross-section, respectively. It should be noted that the ratio of k is a nominal value and reflects the beam–column linear stiffness ratio of the composite frame in the elastic stage generally.

Table 1 lists the details of each composite frame specimen, where h, b_f, t_w, and t_f are the overall height, overall width, web thickness and flange thickness of the I-beam respectively, as shown in Fig. 3; Where b is the width of ring and is determined by AIJ [28]; b_s is the width of beam flange. B and t_s are the overall dimension and thickness of the square steel tube, respectively. The width-to-thickness ratio of the square tubes is less than the limit given in Uy and Bradford [29]

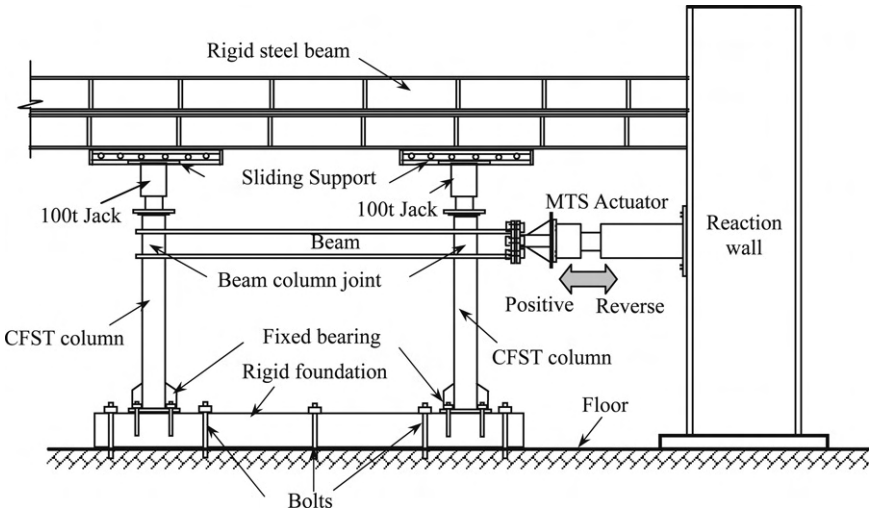

(a) Arrangement of test set-up.

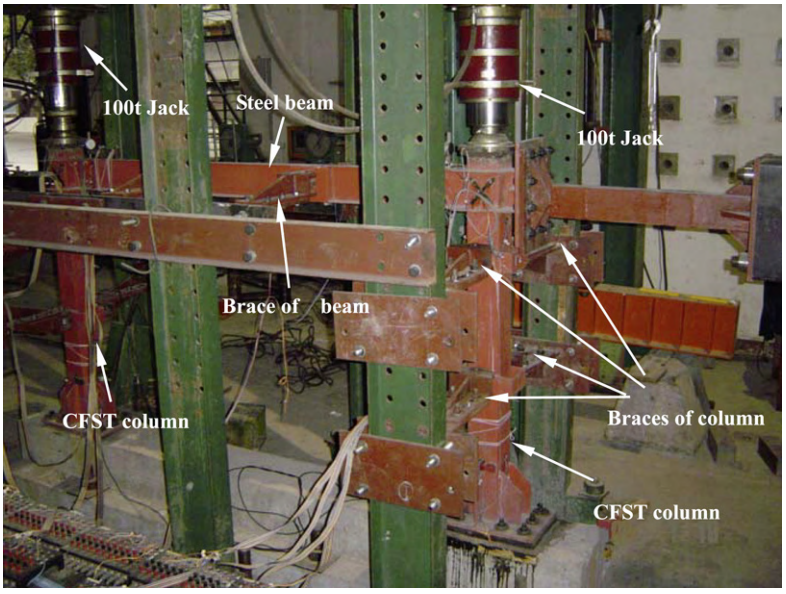

(b) Arrangement of transverse braces.

Fig. 2. Arrangement of test set-up of frame.

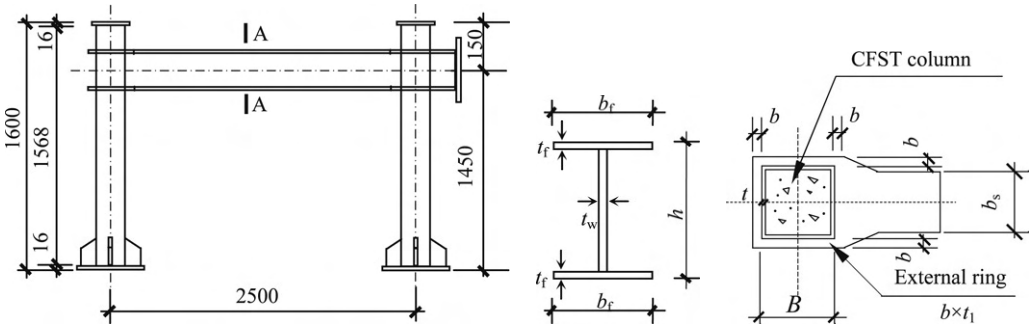

(a) Frame elevation. (b) A-A. (c) Fabrication of joints.

Fig. 3. Frame configuration (Unit: mm).

beyond which local buckling would occur. Table 1 also gives the beam–column linear stiffness ratio, width of the ring, the axial load N_o and axial load level n ($n = N_o/N_u$) for the CFST columns.

Table 1
Summary of frame specimen information

Specimen number	Specimen size (mm)			Beam–column stiffness ratio k	N_o (kN)	Axial Load level n	P_{ue} (kN)	Δ_y (mm)	E_a (kN m)	P_{ua} (kN)	$\frac{P_{ua}}{P_{ue}}$	μ
	Specimen section		Length									
SF-11	column	□120 × 3.46	1450	0.62	50	0.05	106.11	17.66	76.44	109.09	1.028	4.64
	beam	160 × 80 × 3.44 × 3.44	2500									
SF-12	column	□120 × 3.46	1450	0.62	285	0.3	102.75	17.18	68.43	102.27	0.995	4.50
	beam	160 × 80 × 3.44 × 3.44	2500									
SF-13	column	□120 × 3.46	1450	0.41	570	0.6	88.50	15.47	47.47	69.43	0.785	4.71
	beam	140 × 70 × 3.44 × 3.44	2500									
SF-21	column	□140 × 4.00	1450	0.55	50	0.04	166.65	17.77	69.55	164.99	0.990	3.56
	beam	180 × 80 × 4.34 × 4.34	2500									
SF-22	column	□140 × 4.00	1450	0.55	375	0.3	154.11	14.89	52.72	158.84	1.031	3.97
	beam	180 × 80 × 4.34 × 4.34	2500									
SF-23	column	□140 × 4.00	1450	0.34	750	0.6	133.01	9.39	29.11	107.77	0.810	3.56
	beam	160 × 80 × 3.44 × 3.44	2500									

Note: Beam's section parameters are in the sequence of $h \times b_f \times t_w \times t_f$, and column's section is defined by $B \times t_s$.

Table 2
Material properties of steel

Steel type	t (mm)	f_y (N/mm^2)	f_u (N/mm^2)	E_s (N/mm^2)	ν_s	Specimens
SHS tube	3.46	404.0	510.5	2.064×10^5	0.278	SF-11, SF-12, SF-13
	4.00	361.0	433.8	2.062×10^5	0.261	SF-21, SF-22, SF-23
Steel I beam	3.44	303.0	440.9	2.061×10^5	0.262	SF-11, SF-12, SF-13, SF-23
	4.34	361.6	495.5	2.042×10^5	0.262	SF-21, SF-22

3.2. Material properties

The hollow steel tubes were made of cold-formed steel tube. The steel beams and the external ring with the same thickness as the beam were manufactured from mild steel sheet, with three plates being cut from the sheet, tack welded into a I-shaped cross-section and then welded with a single bevel butt weld at the corners. All welded seam is 3 mm thick.

Three tensile coupons cut from the steel tubes and sheets (used to make the beams) were tested to determine the yield stress (f_y), the ultimate tensile strength (f_u), the modulus of elasticity (E_s) and the Poisson's ratio (ν_s). The measured average yield stress, the ultimate tensile strength, the modulus of elasticity and the Poisson's ratio are listed in Table 2.

Self-consolidating concrete (SCC) mix was designed for compressive cube strength (f_{cu}) at 28 days of approximately 42.7 N/mm^2. The measured modulus of elasticity (E_c) of concrete was on average 33,800 N/mm^2. In all the concrete mixes, the fine aggregate used was silica-based sand and the coarse aggregate was carbonate stone. The measured average concrete cube strength of each specimen at the time of the frame test is 52.6 N/mm^2.

Before the pouring of the concrete, the ends of the steel tubes were cut and machined to the required length. Each tube was welded to a square steel base plate of 16 mm thick. The SCC was poured from the top of the steel tube without any vibration. The specimens were placed upright to air-dry. During curing, a very small amount of longitudinal shrinkage of 0.7 to 0.9 mm or so occurred at the top of the column. A high-strength concrete was used to fill this longitudinal gap so that the concrete surface was flush with the steel tube at the top. Each tube was welded to a square steel cover plate of 16 mm thick in order that the axial force transferred from the steel jacket to the steel tube and concrete at the same time in experiment.

3.3. Cyclic loading apparatus

The axial load (N_o) of columns was applied and maintained constant by a 1000 kN capacity hydraulic ram. The hydraulic pump was fixed to the sliding support, as shown in Fig. 2(a), which allowed the specimen to move freely in-plane. This ensured that the column axial load was always concentric. Precautions were made to avoid any eccentricity in the axial load application by very careful alignment of the test setup.

The lateral cyclic load was applied at the end of the steel beam for CFST frame specimens. The frame specimen was a sway frame with rigid connection to the foundation. The bottoms of two columns were fixed through the rigid foundation beam which was fixed to the floor with bolts. To prevent unexpected instability and lateral torsional buckling of the specimen, lateral braces were arranged as shown in Fig. 2(b).

The lateral loading history of frame was generally based on ATC-24 [30] guidelines for cyclic testing of structural steel components. Han et al. [31] used the same loading history in the cyclic tests of CFST members. The loading history included elastic cycles and inelastic cycles. The elastic cycles were conducted under displacement control at displacement levels of $0.25\Delta_y$, $0.5\Delta_y$ and $0.7\Delta_y$, where Δ_y is the estimated lateral

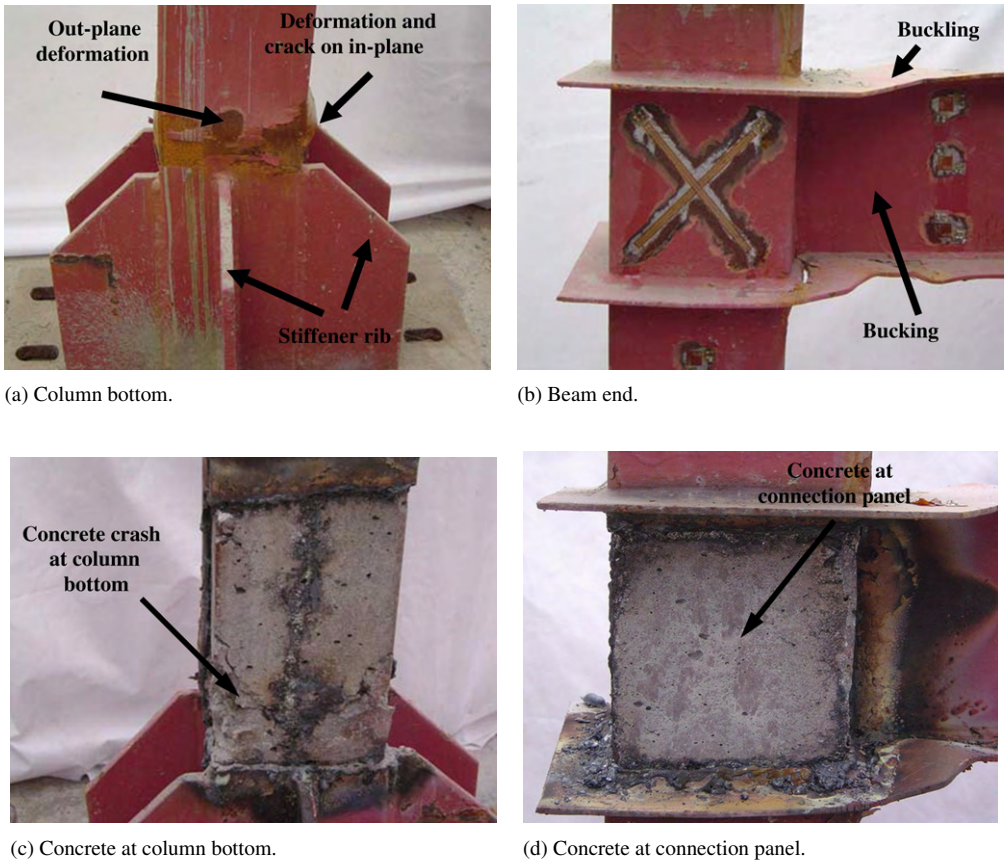

(a) Column bottom.

(b) Beam end.

(c) Concrete at column bottom.

(d) Concrete at connection panel.

Fig. 4. Typical failure mode of the composite frames (SF-13).

yielding displacement corresponding to the lateral yielding load P_y. The P_y was assumed to be $0.7P_u$, where P_u is the estimated ultimate lateral loading capacity calculated using the previously described FEA modeling in this paper. Two cycles were imposed at each of the lateral displacement levels of $0.25\Delta_y$, $0.5\Delta_y$ and $0.7\Delta_y$. The inelastic cycles were then taken to lateral displacement levels of Δ_y, $1.5\Delta_y$, $2\Delta_y$, $3\Delta_y$, $5\Delta_y$, $7\Delta_y$ and $8\Delta_y$. Three cycles were imposed at each displacement levels of Δ_y, $1.5\Delta_y$ and $2\Delta_y$; two cycles were imposed at each additional inelastic displacement level described above.

3.4. Test results and discussion

3.4.1. Failure modes

It was found that, the composite frames had a similar failure mode and failed in the strong-column–weak-beam mode. There were obvious buckling deformation at the beam end and the column bottom, as shown in Fig. 4(a)–(d). At the bottom of the outer steel of CFST columns there appeared obvious deformation and crack in the loading plane, as shown in Fig. 4(a), but there was slight out-of-plane deformation. The center of the plastic hinge in the column is located about 30 mm away from the fastened plate. The core concrete crash was absent after the test, as shown in Fig. 4(c). The plastic hinge of beam end locates at a distance about 30 mm away from the ring, as shown in Fig. 4(b). The core concrete of connection panel has good integrity without obvious cracks or deformation, as shown in Fig. 4(d). The enhanced structural behaviour can be explained in terms of "composite action" between the steel tube and its core concrete.

All the frames had four plastic hinges, two of them at the beam end, two of them at the column bottom. The first plastic hinge was observed at beam end near the MTS actuator, and the second hinge occurred at the end of the beam. The hinges on columns were formed after the beam hinges, as shown in Fig. 5.

3.4.2. Lateral load (P) versus lateral displacement (Δ)

The recorded curves of lateral load (P) versus lateral displacement (Δ) of the composite frames are shown in Fig. 6. The test results showed that the lateral load (P) versus lateral displacement (Δ) hysteretic curves of the composite frames were plump shuttle shape. The curves have no obvious strength and stiffness degradation. The maximum loads (P_{ue}) obtained from the curves are listed in Table 1.

Fig. 7 shows the lateral load (P) versus lateral displacement (Δ) envelop curves of the two group composite frames. It can be seen that the axial load level (n) influences not only the ultimate lateral load (P_{ue}) but also ductility of the composite frames in general.

Specimen SF-22 was selected to show the typical lateral load (P) versus lateral displacement (Δ) envelop curve of the tested specimens in Fig. 8. It can be found from Fig. 8 that, there are generally four typical loading stage of the composite frame, the four points in Fig. 8 represent different stages during the

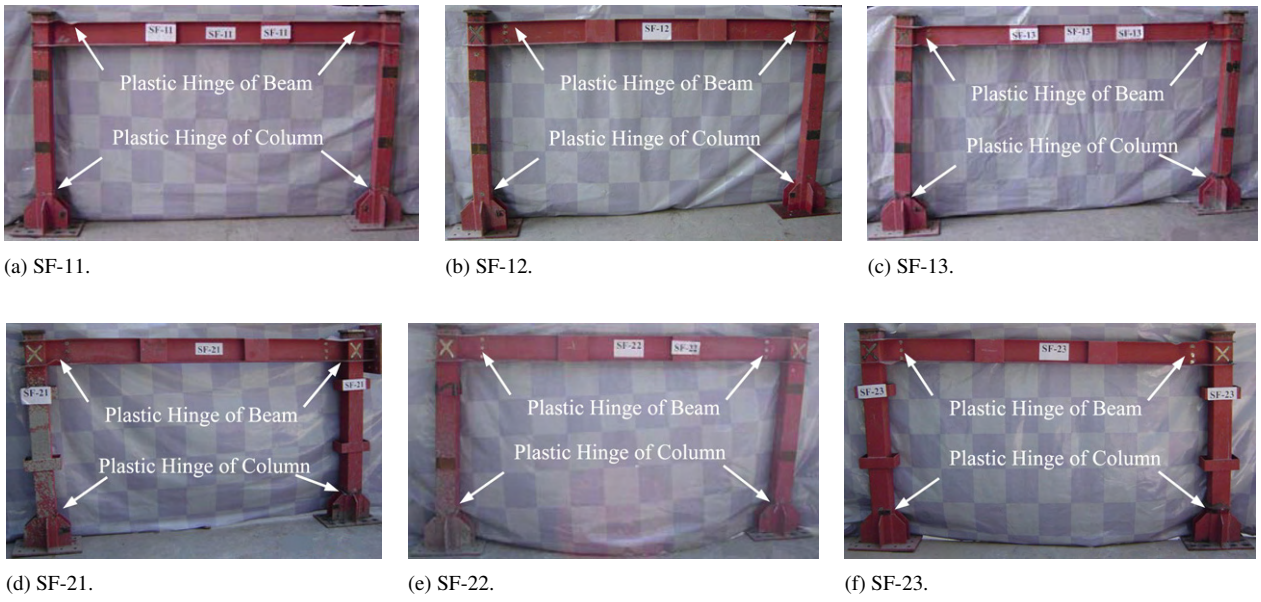

(a) SF-11. (b) SF-12. (c) SF-13.

(d) SF-21. (e) SF-22. (f) SF-23.

Fig. 5. Frame specimen failure mode.

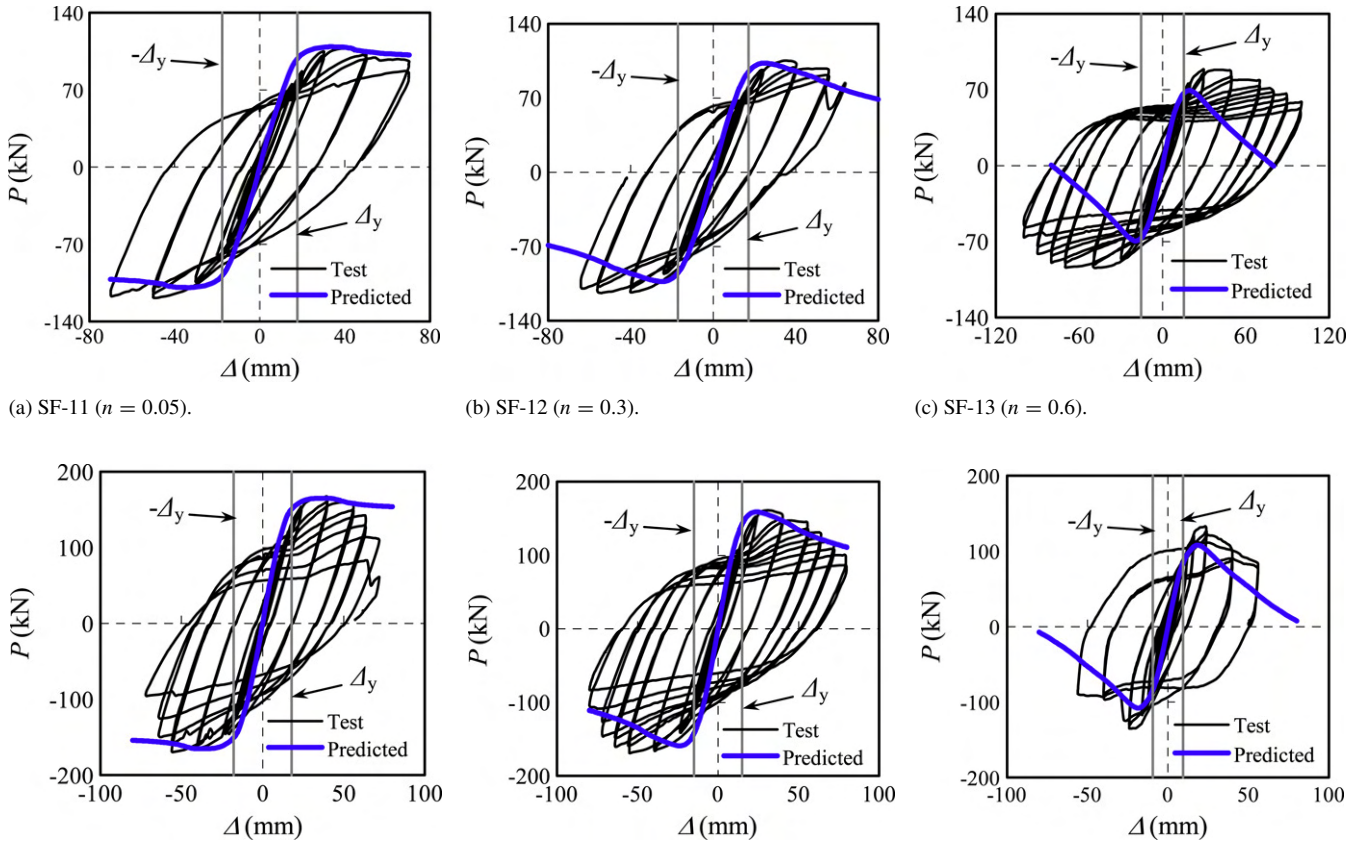

(a) SF-11 ($n = 0.05$). (b) SF-12 ($n = 0.3$). (c) SF-13 ($n = 0.6$).

(d) SF-21 ($n = 0.04$). (e) SF-22 ($n = 0.3$). (f) SF-23 ($n = 0.6$).

Fig. 6. Cyclic load (P) versus lateral deflection (Δ) of tested composite frames.

incremental lateral load. Point 1 corresponds to the stage when the extreme fibers of steel beam start to yield due to the moment of test frame. The composite frame is in elastic stage before point one. Point 2 refers to the stage when the compression fiber of CFST steel columns reaches its yield stress. The steel beam section starts to yield and the yielding area of the compression zone of CFST columns gradually increases, and the composite frame begins to start elastic–plastic stage after point one. Point 3 shows the ultimate lateral load (P_{max}) of the composite frame. The curve descends from point 3. Point 4 is the stage when the

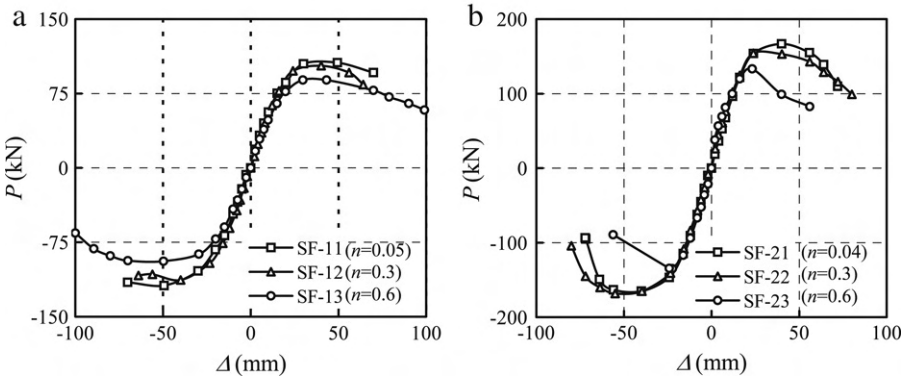

Fig. 7. Lateral load (P) versus displacement (Δ) envelope curves.

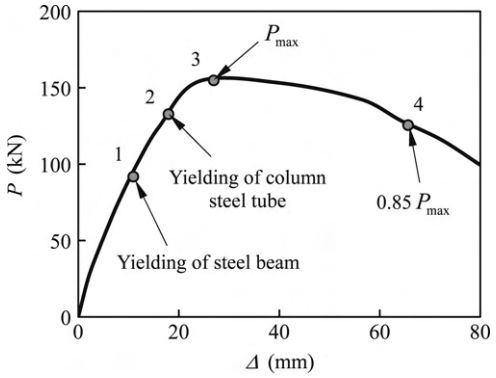

Fig. 8. Typical P versus Δ envelop curve (SF-22).

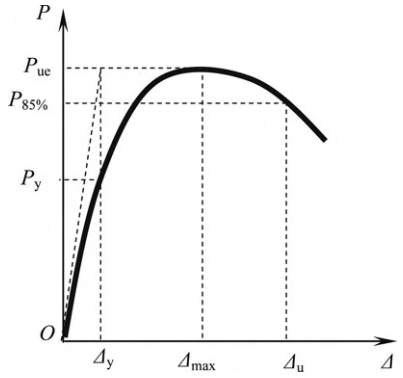

Fig. 10. Determination for yield point of specimens.

load reaches 85% of the ultimate load P_{max}. This means that the frame approximately reaches failure limit, if the point defined is at the ultimate state, in general.

3.4.3. Dissipated energy ability and ductility coefficient

Typically, recorded lateral load to deflection relationship may be simplified as shown in Fig. 9. From this simplification, Eq. (1) may be used to calculate the dissipated energy ability (E_a) according to the Chinese Standard JGJ 101-96 [32].

$$E_a = \frac{S_{ABC} + S_{CDA}}{S_{OBE} + S_{ODF}}, \tag{1}$$

where S_{ABC} and S_{CDA} are the areas under curves ABC and CDA as shown in Fig. 9(a), S_{OBE} and S_{ODF} are the areas within the triangles OBE and ODF as shown in Fig. 9(b).

Table 1 shows the ductility coefficient (μ) and the energy dissipation (E_a) of all composite frames, respectively. While the ultimate load is reduced evidently at a higher axial load level, the ductility of the frame also decreased slightly. In this paper, ductility is measured by the ductility coefficient $\mu(=\Delta_u/\Delta_y)$ where Δ_y is the lateral displacement at material yield and Δ_u the lateral displacement when the lateral load falls to 85% of the maximum lateral strength (P_{ue}). Δ_y and Δ_u are determined according to Fig. 10 from JGJ 101-96 [32]. As expected, Table 1 indicates that: (1) In general, the axial load level (n) had influence on the total dissipated energy ability (E_a) of the specimens, i.e. E_a decreased obviously with increasing axial load level for frames. (2) The beam–column stiffness ratio level (k) also had influence on the total dissipated energy ability (E_a) of the frames, i.e. E_a increased with increasing beam–column stiffness ratio. (3) Generally, the ultimate lateral load (P_{ue}) increases with an increase in the beam–column linear stiffness ratio (k) within the scope of these tests under the same axial load level (n). The beam–column

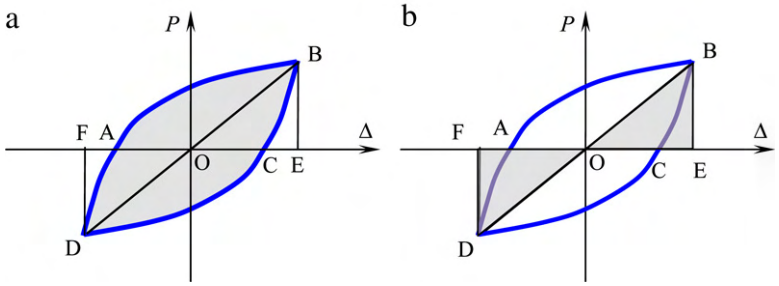

Fig. 9. Idealized P–Δ hysteretic relationship.

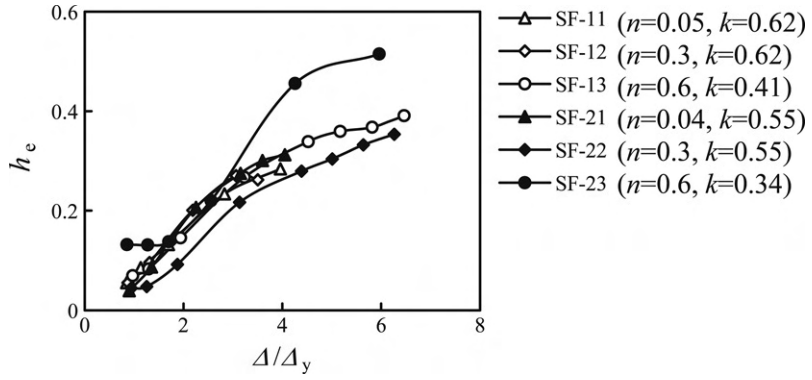

Fig. 11. h_e–Δ/Δ_y curves.

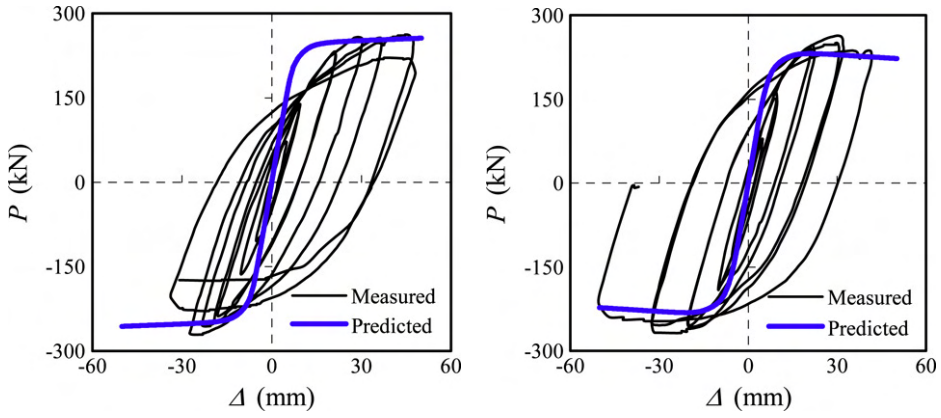

(a) 15-SCP. (b) 30-SCP.

Fig. 12. Comparison of load versus displacement curves between predicted and experimental results [8].

linear stiffness ratio was changed within a limited extent and it was varied in relation to the other parameters and hence conclusions were useable relatively.

3.4.4. Damping coefficient

The equivalent damping coefficient (h_e) can be defined as

$$h_e = \frac{E_a}{2\pi}. \tag{2}$$

Fig. 11 demonstrates that the accumulative equivalent damping coefficient (h_e) of frames increases greatly with the increasing relative displacement (Δ/Δ_y). Axial load level (n) has some effect on the h_e–Δ/Δ_y relationship, with higher axial load level tending to slightly increase the equivalent damping coefficient for frames. The beam–column linear stiffness ratio (k) has moderate influence on the h_e.

4. Verification of FEA model

All the calculated monotonic P–Δ curves of composite frames of this paper by ABAQUS are also given in Figs. 6 and 12. The FE curves matched well with the envelop curve of cyclic lateral load (P) versus lateral displacement (Δ) relationships by experimental results. The main reason is the excellent plastic performance of CFST members. The favorable confined effect of core concrete by steel tube makes the cumulate damage of concrete in CFST member become inconspicuous.

The lateral load (P) versus lateral displacement (Δ) curves of the test frames obtained from FEM model are plotted in Fig. 13 together with the experimental envelop curves of composite frames. It can be seen that generally good agreement has been achieved between experimental curves and numerical curves using FEM model.

The ultimate lateral loads of composite frames obtained from the test (P_{ue}) and finite element analysis by ABAQUS (P_{ua}) as well as the load–displacement curves have been investigated. Table 1 shows a comparison of the ultimate loads of the composite frames obtained experimentally and numerically using FEM model. It can be seen that good agreement has been achieved between the two sets of results for most of the composite frames except for those composite frames tested under an axial load level of 0.6. It is expected that, higher axial load level means higher axially compressive load, this may increase the effects of the imperfections, such as the possibly unexpected fabrication imperfections of the testing setup, and the initially compressive load eccentricity of the composite columns.

It should be noted that, there were seldom experimental results on beam to concrete-filled steel tubular column frames had been published in the past. Thus only the test results presented in this paper was used to verify the FEM model. The

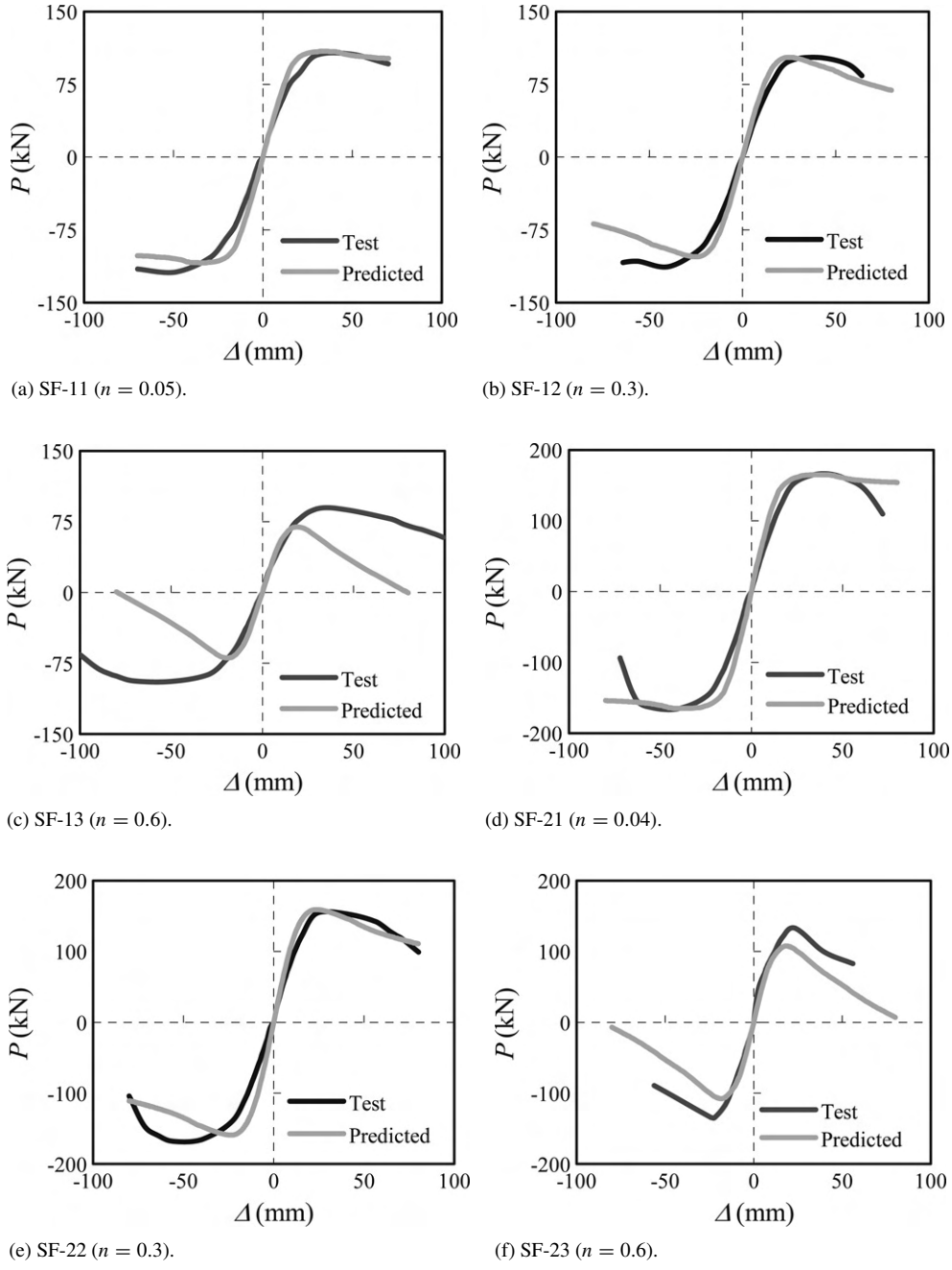

(a) SF-11 ($n = 0.05$). (b) SF-12 ($n = 0.3$).

(c) SF-13 ($n = 0.6$). (d) SF-21 ($n = 0.04$).

(e) SF-22 ($n = 0.3$). (f) SF-23 ($n = 0.6$).

Fig. 13. Comparisons of lateral load versus displacement curves.

feasibility of the model with expanded specimen parameters needs to be verified further. The FEM model established based on ABAQUS in this paper can be used conveniently to analyze the interaction between the steel and the concrete. The analytical results by using the FEM model will be presented in another accompanying paper.

5. Conclusions

From the results of this paper, the following conclusions may be drawn within the limitations of the research:

(1) The experiment shows that CFST frame has excellent earthquake resistance. The composite CFST frames were designed based on the weak-beam–strong-column strategy. Beam failure was observed first in all the frames.

(2) The lateral load carrying capacity, ductility coefficient and energy dissipation of composite frame decreased as the axial load level in the column increases. The ultimate lateral load of composite frame increases with an increase in beam–column linear stiffness ratio if other conditions are kept the same.

(3) The FE modeling developed in this paper was able to reasonably predict the lateral load versus lateral displacement relationship of composite frame, and the ultimate lateral load carrying capacity.

Acknowledgements

The research reported in this paper is part of the Project 50425823 supported by the National Natural Science Foundation of China, the project supported by the Start-Up Fund for Outstanding Incoming Researchers of Tsinghua University, and the Tsinghua University & ZhongDa Group Postdoctoral Science Foundation. Their financial support is highly appreciated.

References

[1] Shams M, Saadeghvaziri MA. State of the art of concrete-filled steel tubular columns. ACI Structural Journal 1997;94(5):558–71.
[2] Shanmugam NE, Lakshmi B. State of the art report on steel–concrete composite columns. Journal of Constructional Steel Research 2001; 57(10):1041–80.
[3] Gourley BC, Tort C, Hajjar JF, Schille RA. A synopsis of studies of the monotonic and cyclic behaviour of concrete-filled steel tube beam–columns. Report no. ST1-01-4 (Version 3.0). Department of Civil Engineering, University of Minnesota; 2001.
[4] Nishiyama I, Morino S, Sakino K, et al. Summary of research on concrete-filled structural steel tube column system carried out under the US–Japan cooperative research program on composite and hybrid structures. BRI research paper no. 147. Japan: Building Research Institute; 2002.
[5] Zhao XL, Grzebieta RH. Void-Filled SHS beams subjected to large deformation cyclic bending. Journal of Structural Engineering, ASCE 1999;125(9):1020–7.
[6] Elchalakani M, Zhao XL, Grzebieta RH. Concrete-filled steel tubes subjected to constant amplitude cyclic pure bending. Engineering Structures 2004;26(14):2125–35.
[7] Elchalakani M, Zhao XL, Grzebieta RH. Variable amplitude cyclic pure bending tests to determine fully ductile section slenderness limits for cold-formed CHS. Engineering Structures 2006;28(9):1223–35.
[8] Kawaguchi J, Morino S, Sugimoto T. Elasto-plastic behaviour of concrete-filled steel tubular frames. In: Composite construction in steel and concrete III, Proceedings of an engineering foundation conference; 1997. p. 272–81.
[9] Matsui C. Strength and behaviour of frames with concrete filled square steel tubular columns under earthquake loading. In: Proceeding of 1st international speciality conference on concrete filled steel tubular structures; 1985. p. 104–11.
[10] Tsai KC, Weng YT, Lin ML. Pseudo dynamic tests of a full-scale CFT/BRB composite frame: Displacement based seismic design and response evaluations. In: Proceeding of the international workshop on steel and concrete composite constructions; 2003.
[11] Muhummud T. Seismic design and behaviour of composite moment resisting frame constructed of CFT columns and WF beams. Ph.D. dissertation. Bethlehem (PA, USA): Department of Civil and Environmental Engineering, Lehigh University; 2003.
[12] Herrera R. Seismic behaviour of concrete filled tube column-wide flange beam frames. Ph.D. dissertation. Bethlehem (PA, USA): Department of Civil and Environmental Engineering, Lehigh University; 2005.
[13] Schneider SP. Axially concrete-filled steel tubes. Journal of Structural Engineering, ASCE 1998;124(10):1125–38.
[14] Hu HT, Huang CS, Wu MH, Wu YM. Nonlinear analysis of axially loaded concrete-filled tube columns with confinement effect. Journal of Structural Engineering, ASCE 2003;129(10):1322–9.
[15] Hu HT, Huang CS, Chen ZL. Finite element analysis of CFT columns subjected to an axial compressive force and bending moment in combination. Journal of Constructional Steel Research 2005;61(12): 1692–712.
[16] Ellobody E, Young B. Design and behaviour of concrete-filled cold-formed stainless steel tube columns. Engineering Structures 2006;28(5): 716–28.
[17] Han LH, Yao GH, Tao Z. Performance of concrete-filled thin-walled steel tubes under pure torsion. Thin-Walled Structures 2007;45(1):24–36.
[18] Hibbitt, Karlson & Sorensen Inc. ABAQUS/standard user's manual, Version 6.5. Providence (RI): Hibbitt, Karlsson, & Sorensen, Inc.; 2005.
[19] Abdel-Rahman N, Sivakumaran KS. Material properties models for analysis of cold-formed steel members. Journal of Structural Engineering, ASCE 1997;123(9):1135–43.
[20] Sully RM, Hancock GJ. Behaviour of cold-formed SHS beam–columns. Journal of Structural Engineering, ASCE 1996;122(3):326–36.
[21] Han LH, Yao GH, Tao Z. Behaviours of concrete-filled steel tubular members subjected to combined loading. Thin Walled Structures 2007; 45(6):600–19.
[22] ACI 318. Building code requirements for structural concrete and commentary. Detroit (USA): American Concrete Institute; 2005.
[23] Lubliner J, Oliver J, Oller S, Oñate E. A plastic-damage model for concrete. International Journal of Solids and Structures 1989;25(3): 299–326.
[24] Lee J, Fenves GL. Plastic-damage model for cyclic loading of concrete structures. Journal of Engineering Mechanics, ASCE 1998;124(8): 892–900.
[25] Hillerborg A, Modeer M, Petersson PE. Analysis of crack formation and crack growth in concrete by means of fracture mechanics and finite elements. Cement and Concrete Research 1976;6:773–82.
[26] Wang WD, Han LH, Tao Z. Experimental research on seismic behaviour of concrete-filled CHS and SHS columns and steel beam planar frames. Journal of Building Structures 2006;27(3):48–58 [in Chinese].
[27] Eurocode 4. Design of composite steel and concrete structures-Part 1.1 General rules and rules for buildings. Brussels (Belgium): European Committee for Standardization, BS EN 1994-1-1:2004.
[28] AIJ. Recommendations for design and construction of concrete filled steel tubular structures. Tokyo (Japan): Architectural Institute of Japan (AIJ); 1997.
[29] Uy B, Bradford MA. Local buckling of cold formed steel in composite structural elements at elevated temperatures. Journal of Constructional Steel Research 1995;34(1):53–73.
[30] ATC-24. Guidelines for cyclic seismic testing of components of steel structures. Redwood City (CA): Applied Technology Council; 1992.
[31] Han LH, Huang H, Tao Z, Zhao XL. Concrete-filled double skin steel tubular (CFDST) beam–columns subjected to cyclic bending. Engineering Structures 2006;28(12):1698–714.
[32] JGJ101-96. Specification for test methods of seismic buildings. Peking: Architecture industrial press of China; 1997 [in Chinese].